ISSN 1027-5495. Functional Materials, 32, No.4 (2025), p. 650-656
doi:http://dx.doi.org/10.15407/fm32.04.650

Modified top-seeding solution growing of $KTaO_3$

G.Yu. Rudko, T.V. Sonko, O.Y. Gudymenko, O.M. Hreshchuk, I.P. Vorona, V.M. Dzhagan, V.O. Yukhymchuk

V. Lashkaryov Institute of Semiconductor Physics, NAS of Ukraine, Kyiv, Ukraine

Received July 18, 2025

The setup for growing single-crystal high-melting-point oxides using top-seeded solution growth method was modified to provide controlled regulation of the crucible bottom temperature. The modified setup was used for growing bulk $KTaO_3$ single crystals, a material with a unique combination of high dielectric constant and other properties in demand in various fields including electronic and optical industries as well as the development of highly sensitive and compact radio-spectroscopic instruments. The quality of $KTaO_3$ single crystals grown in the modified setup was analyzed by several methods, and high crystallinity and purity of the samples were demonstrated.

Keywords: Potassium tantalite, modified growth procedure, incipient ferroelectric, lattice dynamics, crystallinity, purity.

Модифікований метод вирощування $KTaO_3$ із розплаву з використанням верхньої затравки. *Г.Ю. Рудько, Т.В. Сонько, О.Й. Гудименко, О.М. Грещук, І.П. Ворона, В.М. Джаган, В.О. Юхимчук*

Установка для вирощування монокристалічних оксидів з високими температурами плавлення була модифікована з метою забезпечити можливість контролю температури дна тигля. В цій модифікованій установці з використанням верхньої затравки були вирощені монокристали оксиду $KTaO_3$, який характеризується дуже високим значенням діелектричної сталої, що, в комбінації з іншими унікальними властивостями, робить цей матеріал актуальним для застосувань в багатьох областях, включаючи оптичну та електронну промисловості, зокрема, для виготовлення високочутливих і компактних радіоспектроскопічних приладів. Якість вирощених за допомогою модифікованої установки монокристалів $KTaO_3$, була протестована з використанням серії методик, і була продемонстрована висока ступінь кристалічності і чистоти вирощених монокристалів.

1. Introduction

Potassium tantalate, $KTaO_3$, is a member of the family of all-inorganic perovskite dielectrics that exhibit a variety of properties suitable for various applications. In particular, $KTaO_3$ has a unique combination of characteristics that are of both fundamental and practical interest.

In terms of electrical properties, the material, on the one hand, is an perfect insulator due to its high permittivity values [1]; on the other hand, $KTaO_3$ exhibits rather intriguing behavior of incipient ferroelectric, which, when cooled to low temperatures, never reaches a phase transition and retains paraelectric properties (the so-called quantum paraelectric behavior) [2]. Due to these specific electric features, $KTaO_3$ is believed to be a promising material to creating voltage-tunable microwave devices for low-loss tunable filters [3], field-effect transistors [4], etc. Recently, the discovery of superconductivity in the electron gas formed at the interface between crystalline $KTaO_3$ and an insulating overlayer [5] caused a new wave of research interest in $KTaO_3$.

Regarding optical properties, it should be noted that $KTaO_3$ meets various standards of the optical industry. It has a refractive index of 2.381 at 405 nm and a transparency window from 345 to 3000 nm [6]. In terms of processability, single crystalline potassium tantalite is resistant to cleavage and its hardness is almost isotropic; therefore, it can be processed almost in the same way as homogeneous isotropic materials (e.g., optical glass). In view of these advantages, bulk $KTaO_3$ has been used for the production of solid immersion lenses with a high numerical aperture for near-field optical disk systems [7], and, as a component of a solid solution, for electro-optic beam scanners [8, 9]. Also, bulk single crystals are used to produce laser modulators, and digital deflectors [10, 11]. Moreover, $KTaO_3$ possesses a large absorption coefficient in the UV range, which can ensure high photosensitivity.

Another important area of application of bulk $KTaO_3$ crystals is related to the production of dielectric resonators for radio-spectroscopic measurements. Since the pioneering work [12], where $KTaO_3$ ferroelectric resonator was used in EPR spectrometer and a 10-fold improvement in the signal-to-noise ratio was achieved, the idea has been repeatedly addressed by radio-spectroscopists (see, e.g. [13, 14]). To achieve high functional characteristics of these resonators, the crucial issue is the quality of single crystals.

Thus, in view of the numerous applications of $KTaO_3$, the growth of high-quality single crystals is of continuing interest; existing techniques for growing this material are constantly being improved, and new ones are emerging.

At present, two groups of methods for growing bulk $KTaO_3$ single crystals are predominantly used. The methods related to the first group imply pulling an ingot out of a melt. Representatives of this group include modified Czochralski and Kyropolis methods, as well as top-seeding solution growth [15–19]. The methods of the other group are based on spontaneous crystallization from a melted solution [20, 21].

The method of top-seeding solution growth (TSSG) is used more frequently than other techniques and provides larger single crystals. This method can be described as a combination of the Czochralski technique with the procedure of growing from a melted solution. The procedure of TSSG was developed for the special case of growing single crystals of substances with very high melting temperatures; the main idea is to growing at temperatures lower than the melting point of the targeted crystal. To downshift the growth temperature, the crystals are grown not from the melt of the targeted material itself (like in Czochralski method) but from a molten solution of this material; e.g., in our case, when the targeted material is $KTaO_3$, the solvent is K_2O. To obtain high-quality single crystals using the TSSG method, special attention must be paid to the requirements imposed on this method. These include: the correct selection of the composition of the molten solution, control of the temperature distribution inside the furnace, and maintaining proper convection streams in the molten solution inside the crucible. Other growth details, such as optimization of the pulling rate, correct choice of size, shape and orientation of the seed crystal face, etc., are common for all Czochralski-related methods and must also be carefully considered. In view of the above, the improvement of TSSG method is constantly in progress and, despite considerable achievements, there is still a vast field of options for the optimization of the technique.

The goal of the present paper is to introduce improvements beyond the present status of the top-seeded solution-growth method; for this purpose, we modify the growth setup aiming to reduce temperature gradients within the crucible. The modified setup is tested by growing $KTaO_3$ single crystals and confirming their high quality through careful characterization using several methods.

2. Experimental results

2.1. Procedure for growing bulk $KTaO_3$

$KTaO_3$ single crystals were grown by a modified TSSG method in ambient atmosphere. The feed material for growth was a two-component melt-solution system K_2O-$KTaO_3$, where K_2O is the solvent. The crystal growing setup used for growing $KTaO_3$ is shown schematically in Fig. 1, a,b. The heating of the melt solution is provided by radio-frequency heaters (the inductor). The platinum crucible is placed inside the inductor and mounted on the alumina tube which can withstand temperatures up to 1500 °C. Radio-frequency currents in the heater induce the currents in the conductive crucible and thus heat the crucible while inside the crucible the melt-solution is heated via thermal conductiv-

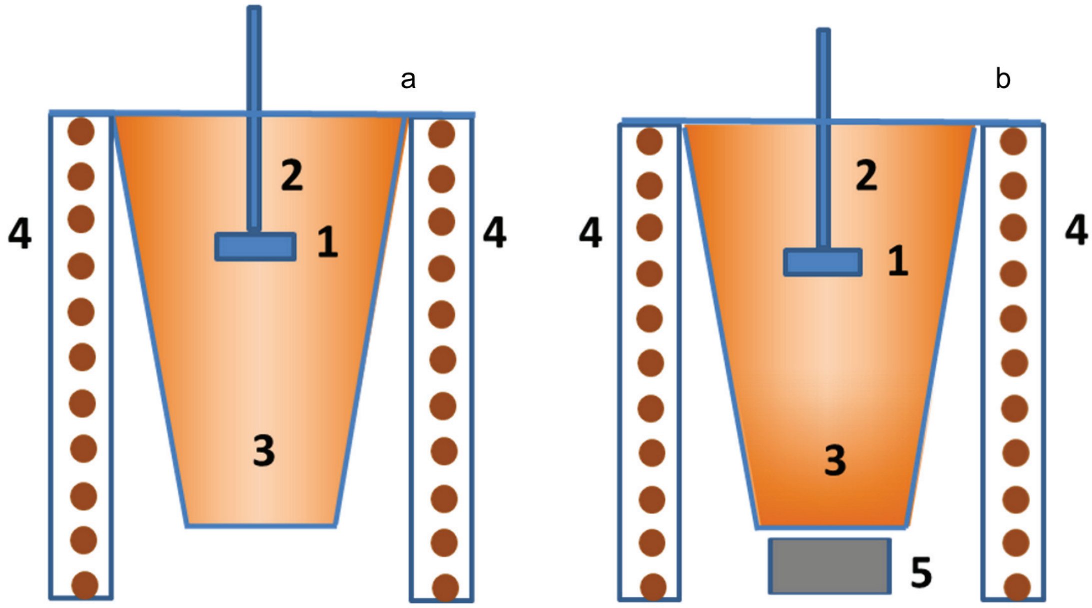

Fig. 1. Schematic cross-section of the modified crystal-growing setup. 1 – crystal seed that is mounted on a moveable pull rod 2; 3 – crucible; 4 – inductor (radio-frequency heater); 5 – ferrite bar. a) – without ferrite bar; b) ferrite bar is partially introduced into the inductor. Changes in the color filling of the crucible in Fig. 1, b reflect the increasing temperature of the melt-solution in the lower part of the crucible.

ity processes. Therefore, the temperature of the walls of the platinum crucible is higher than the temperature in the central parts of the crucible; besides, the temperature of the walls is higher than the temperature of the crucible bottom, see Fig. 1, a.

To ensure more homogeneous heating of the solution-melt inside the crucible, we applied additional heating of the crucible bottom. To tune the temperature of the crucible bottom, a ferrite bar was used, which was inserted into the inductor, as shown in Fig. 1, b. The position of this ferrite bar is adjustable, it can be easily moved vertically along the setup axis and fixed in the selected position. The ferrite bar is enveloped by a system of quartz tubes for water-cooling during the growth (not shown in Fig. 1 a, b).

When introduced into the radio-frequency-powered inductor, the ferrite bar concentrates the magnetic field lines and, consequently, induces extra currents in the conducting bottom of the crucible. As a result, the bottom is heated additionally. To optimise the temperature of the bottom, we shift the ferrite bar upward until the bottom of the crucible is as hot as its walls.

Controllable heating of the crucible bottom provides many advantages. Firstly, due to this modification of the growing setup, we avoid spontaneous nucleation of seeds at the bottom of the crucible which can lead to the growth of "stray" $KTaO_3$ crystals. Obviously, the formation of extra seeds is undesirable merely in view of material waste considerations. Beside wasting the source material, growth of "stray" crystals can have even more serious consequences. Indeed, when "stray" crystals that emerge at the bottom become sufficiently large, the growth procedure can be spoiled completely because these unwantable crystals can interconnect with the high-quality ingot that grows from the top seed. An additional advantage of the controllable heating of the crucible bottom is the reduction of temperature gradients, which in turn leads to a decrease in thermal stresses and plastic deformations in the growing ingots [22].

The modified setup shown in Fig. 1 was used for growing $KTaO_3$ single crystals. The starting materials for loading the crucible were K_2CO_3 and Ta_2O_5 in a non-stoichiometric ratio. The growing procedure took place in two steps. The first step was the synthesis of the feed material for growth. The melt-solution had a non-stoichiometric composition. Considering that K_2CO_3 is more volatile than Ta_2O_5 we adjusted the ratio of the components. We started with the ratio of K:Ta of about 1.5 which is known to be the preferable option for spontaneous crystallization growth mode [23]. It was shown experimentally that the optimal coefficient of excess potassium in the starting melt-solution for our growth method is 1.46. If the K:Ta ra-

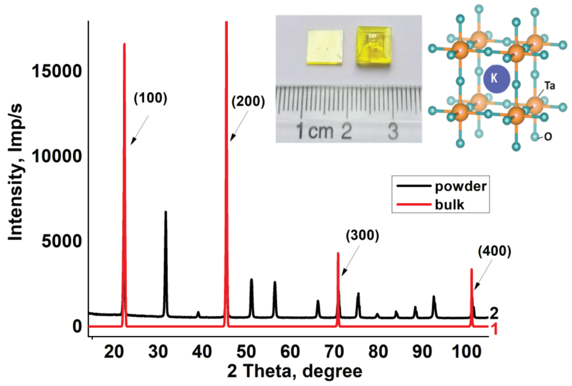

Fig. 2. Diffraction pattern of the non-oriented bulk (1) and powdered (2) $KTaO_3$ samples. Inset: the photo of the bulk single crystal of $KTaO_3$ grown by the modified TSSG method and the plate cut from this ingot; schematic representation of $KTaO_3$ unit cell.

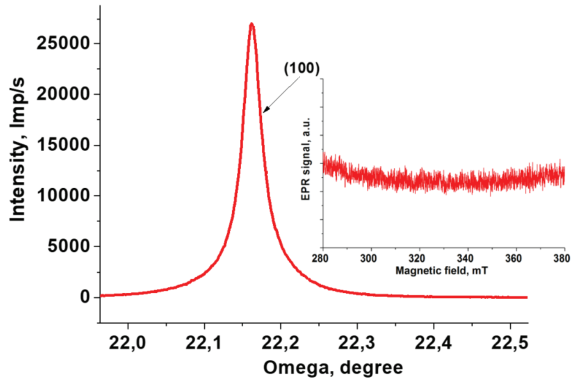

Fig. 3. Diffraction peak of the oriented to the (100) plane $KTaO_3$ sample measured in the high-resolution mode. The inset of this figure shows the EPR spectrum of the grown $KTaO_3$ sample.

tio is higher than 1.46, the crystals are opaque, while too much Ta results in a large number of dislocations in the crystals.

Growth occurrs by pulling the seed from the feed K_2O-$KTaO_3$ material discussed above. This melt-solution is a low-viscosity liquid that is stable against supercooling. The latter property is favorable for growing good crystals since minor random changes in temperature do not lead to the formation of new crystallization centers in the melt-solution inside the crucible. The best quality of single crystals is achieved when the pulling is done without rotating the rod with the attached seed. The pulling speed was varied from 0.5 to 2 mm/hour. The rate of the melt-solution cooling during the growth was 3–10 ^{o}/hour.

After completion of ingot growth, the temperature and pulling speed were increased to safely extract the crystals from the melt-solution. The whole pulling and cooling process lasted for 8–10 hours. The sizes of the crystals grown by our modified technique varied from (3x3x3) mm^3 to (10x8x7) mm^3. The photo of $KTaO_3$ single crystal grown by the above procedure is shown in the inset in Fig. 2.

2.2. XRD characterization of $KTaO_3$

The obtained $KTaO_3$ crystals were examined by X-ray diffraction (XRD) to characterize the crystal structure and quality. XRD experiments were carried out using a Philips X'Pert PRO – MRD diffractometer equipped with a CuKα radiation source (wavelength $\lambda = 0.15406$ nm). The anode voltage of the tube was 45 kV, current 40 mA. Diffraction patterns were registered in the symmetric (2θ/ω) geometry employing either standard or high-resolution mode. The scanning step was 0.025 degrees, time of data acquisition at each point was 1 second.

The diffraction pattern of the powder sample exhibits all reflections of cubic $KTaO_3$ (PDF # 010-77–1133) with the lattice parameter a = 3.9883 Å (black curve (2), Fig. 2). The diffraction pattern of the bulk sample shows only (100), (200), (300) and (400) peaks. The half widths and positions of the peaks (100), (200), (300) and (400) were analyzed by Williamson-Hall method [26, 27]. The estimated values of the average coherence length (D) and microstrains (ε) were ~30.6 nm and 0.12%, respectively. We have also done additional scanning in the high-resolution mode in the direction perpendicular to the diffraction vector (ω-scanning, see. Fig.3). For this purpose a quadruple Ge(220) monochromator and a double Ge(220) analyzer were used. Based on the half-width of the (100) reflection, the average dislocation density was obtained. It does not exceed 1.3×10^5 cm^{-2}. Thus, both normal and high-resolution XRD measurements show that our crystals are of high integrity and good quality.

2.3. Lattice dynamics features of single crystalline $KTaO_3$

Traditional crystallographic studies were supplemented by optical characterization. To get the insight into the lattice dynamics and symmetry, the samples of $KTaO_3$ grown by the modified TSSG method were explored by Raman spectroscopy. The measurements were carried out in the frequency range of 10-800 cm^{-1} using a single-stage spectrometer MDR-23 (LOMO) equipped with a cooled CCD detector (Andor iDus 401, UK). Raman spectra were excited with a 532 nm solid-state laser. The laser power density on the samples was

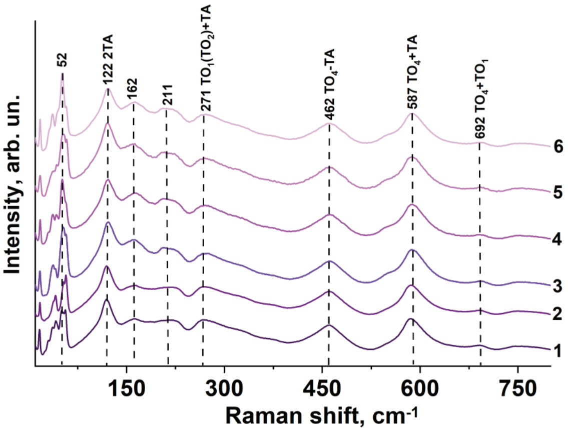

Fig. 4. Raman scattering spectra of $KTaO_3$ registered at different points on the surface. The exciting light wavelength is 532 nm. Dashed lines show the maxima of the most intense bands in the Raman spectra.

less than 10^3 W/cm^2 to preclude any thermal or photoinduced modification of the samples. A spectral resolution of 4 cm^{-1} was determined from the Si phonon peak width of a single crystal Si substrate. The position of the Si phonon peak at 520.5 cm^{-1} was used as a reference for determining the position of the peaks in the Raman spectra.

Fig. 4 shows Raman scattering spectra measured in different points on the surface (crystal growth plane) of the grown $KTaO_3$ single crystal. When analyzing Raman spectra, it should be taken into account that $KTaO_3$ is a cubic crystal (see the crystal cell in the inset of Fig. 2) with one formula unit per unit cell of the lattice. Each ion in the lattice is located at a point of inversion symmetry. Consequently, there are 15 degrees of freedom for vibrations including 3 acoustic (F_{1u}) and 12 optical ($3F_{1u} + F_{2u}$) modes [24]. At the same time, since single-crystalline $KTaO_3$ has an inversion center, only two-phonon processes must be Raman active. Accordingly, all Raman features observed in the spectra (Fig. 4) must be of exclusively second-order nature. They must originate predominantly from the Brillouin zone boundary where the combined density of states tends to be very large. In full agreement with symmetry considerations and known selection rules for the cubic perovskite structure, no first-order Raman features are seen in Fig. 4. The predominant structural features of the spectrum can be interpreted in accordance with [25] as being due to a combination of phonons and overtones between transverse modes. The features in all spectra in Fig. 4 are observed at 271, 462, 587, 692 cm^{-1}. These peaks can be ascribed to the following combinations of phonons: TO_1+TA, TO_2+TA, TO_4-TA, TO_4+TA and TO_4+TO_1, respectively. Note, that the values of TO_1 = 162 cm^{-1} and TO_2 = 211 cm^{-1} obtained from Raman studies are in reasonable agreement with the neutron-diffraction data [15].

As can be seen from Fig. 4, the obtained spectra are almost identical: the frequency positions of the bands and their half-widths practically coincide. These observations indicate that the grown sample is characterized by uniformity of both component composition and crystalline perfection. The latter is also evidenced by a very weak Rayleigh scattering, which allowed recording the Raman spectra starting with 10 cm^{-1}.

2.3. Detection of paramagnetic centers

To further analyze the quality of the samples grown by the modified TSSG method, namely, to find out whether local structural defects and impurities are present in these samples, we conducted EPR experiments. This method provides reliable information about paramagnetic centers (either impurity-related or intrinsic) in the lattice. EPR measurements were carried out using an X band EPR spectrometer “Radiopan”. The sensitivity of the method for center detection was about 10^{-12} spins. As it is seen from the inset in Fig. 3, no EPR sygnals were observed. Thus, within the limits of experimental error, we can state that concentration of paramgnetic centers in our samples is less than ~ 5 x 10^{-12} spins per cm^3 which is an encouraging result for using our crystals for fabrication of dielectric resonators.

3. Conclusions

The procedure of top-seeded solution growth was modified by adding the option of tunable heating of the crucible bottom. By adding this factor of control we were able to reduce temperature gradients inside the crucible and suppress the spontaneous formation of unwanted seeds at the bottom of the crucible. The modified setup was implemented to grow bulk single crystalline potassium tantalate. The crystals were studied by XRD, Raman, and magnetic resonance spectroscopy methods, and the high crystal quality and purity of the samples were proven; thus, the crystals grown using the improved growth setup have broad application prospects.

Acknowledgement

Support by the NASU project "New physical principles and technologies for the development of the element base of modern infrared photoelectronics" (No. 0125U000799) is acknowledged.

References

1. O. Aktas, S. Crossley, M.A. Carpenter, E.K.H. Salje, Polar correlations and defect-induced ferroelectricity in cryogenic $KTaO_3$, Phys. Rev. B. 90 (2014) 165309, https://doi.org/10.1103/PhysRevB.90.165309.
2. C. Ang, A.S. Bhalla, L.E. Cross, Dielectric behavior of paraelectric $KTaO_3$, $CaTiO_3$, and $(Ln_{1/2}Na_{1/2})TiO_3$ under a dc electric field, Phys. Rev. B. 64 (2001) 184104, https://doi.org/10.1103/PhysRevB.64.184104.
3. G.R. Geyer, B. Riddle, J. Krupka, L.A. Boatner, Microwave dielectric properties of single-crystal quantum paraelectrics $KTaO_3$ and $SrTiO_3$ at cryogenic temperatures, J. Appl. Phys. 97 (2005) 104111, https://doi.org/10.1063/1.1905789g.
4. K. Ueno, I.H. Inoue, T. Yamada, H. Akoh, Y. Tokura, H. Takagi, Field effect transistor based on $KTaO_3$ perovskite, Appl. Phys. Lett. 84 (2004) 3726–3728, https://doi.org/10.1063/1.1703841.
5. C. Liu, X. Yan, D. Jin, Y. Ma, H.-W. Hsiao, Y. Lin, T.M.Bretz-Sullivan, X. Zhou, J. Pearson, B. Fisher, J.S Jiang, W. Han, J.-M. Zuo, J. Wen, D. D. Fong, J. Sun, H. Zhou, A. Bhattacharya, Discovery of two-dimensional anisotropic superconductivity at $KTaO_3$ (111) interfaces, Condensed Matter. Science 371 (2021) 716-721, https://doi.org/10.1126/science.aba5511.
6. L. Hu, D. Sun, H. Zhang, J. Luo, C. Quan, Z. Han, K. Dong, Y. Chen, and M. Cheng, Growth, defects, mechanical, and optical properties of transparent $KTaO_3$ single crystal, J. Mater. Sci.: Mater. Electron. 33 (2022) 1–13, https://doi.org/10.1007/s10854-022-08246–1.
7. K. Fujiura, M. Sasaura, $KTaO_3$ Solid Immersion Lens for Nearfield Optical Disk System, NTT Technical Review. 5 (2007), U0052A https://doi.org/10.53829/ntr200709sp4.
8. Y. Tanga, J. Wanga, X. Wanga, D. Baofeng, S. Tanga, J. Foshee, KTN based electro-optic beam scanner, Proc. of SPIE 7135 (2008) 713538, https://doi.org/10.1117/12.802928.
9. J. Foshee, S. Tang, Y. Tang, X. Wang, B. Duan, A Novel High-Speed Electro-Optic Beam Scanner Based on KTN Crystals, Proc. of SPIE 6709 (2007) 670908, https://doi.org/10.1117/12.731286.
10. **X. Wang, X. Mao, P. Chen, Q. Du, Y. Yang, P. Qiao, S. Zhang, Z. Li, R. Zhang, B. Liu, J. Wang, Potassium tantalate niobate crystals: Efficient quadratic electro-optic materials and their laser modulation technology, Journal of Materiomics 9 (2023) 838-854, https://doi.org/10.1016/j.jmat.2023.02.006.**
11. B. Liu, H. Zhang, Y. Zhang, X. Lv, Y. Yang, L. Wei, X. Wang, H. Yu, C. Zhang, J. Li, Growth and Laser Modulation Properties of $KTa_{0.63}Nb_{0.37}O_3$ Single Crystals, Acta Physica Polonica A 135 (2019) 396-400, https://doi.org/10.12693/APhysPolA.135.396.
12. I.N. Geifman, I.S. Golovina, V.I. Kofman, R.E. Zusmanov, The use of ferroelectric material for increasing sensitivity of the EPR spectrometers, Ferroelectrics 234 (1999) 81-88, https://doi.org/10.1080/00150199908225283.
13. E. Vahapoglu, J.P. Slack-Smith, R.C.C. Leon, W.H. Lim, F.E. Hudson, T. Day, T. Tanttu, C.H. Yang, A. Laucht, A.S. Dzurak, J.J. Pla, Single-electron spin resonance in a nanoelectronic device using a global field, Sci. Adv. 7 (2021) eabg9158, https://doi.org/10.1126/sciadv.abg9158.
14. V.V. Nosenko, I.P. Vorona, S.V. Lemishko, I.S. Golovina, V.O. Yukhymchuk, S.M. Okulov, V.B. Neimash, V.Yu. Povarchuk, S.O. Solopan, A.G. Belous, Enhancement of radiation-induced EPR signal in bioapatites, Semiconductor Physics, Quantum Electronics & Optoelectronics 25 (2022) 173–178, https://doi.org/10.15407/spqeo25.02.173.
15. G. Shirane, R. Nathans, V. J. Minkiewicz, Temperature Dependence of the Soft Ferroelectric Mode in $KTaO_3$, Phys. Rev. 157 (1967) 396-399, https://doi.org/10.1103/PhysRev.157.396.
16. H. Uwe, T. Sakudo, Electrostriction and Stress-Induced Ferroelectricity in $KTaO_3$, J. Phys. Soc. Jpn. 38 (1975) 183–189, https://doi.org/10.1143/JPSJ.38.183.
17. Y Fujii, T Sakudo, Dielectric and optical properties of $KTaO_3$, Journal of the Physical Society of Japan 41 (1976) 888-893, https://doi.org/10.1143/JPSJ.41.888.
18. B. Hehlen, A.-L. Perou, E. Courtens, R. Vacher, Observation of a Doublet in the Quasielastic Central Peak of Quantum-Paraelectric $SrTiO_3$, Phys. Rev. Lett. 75 (1995) 2416-2419, https://doi.org/10.1103/PhysRevLett.75.2416.
19. H. Vogt, H. Uwe, Hyper-Raman scattering from the incipient ferroelectric $KTaO_3$, Phys. Rev. B 29 (1984) 1030–1034, https://doi.org/10.1103/PhysRevB.29.1030.

20. B. Salce, J.L. Gravilt, L.A. Boatnert, Disorder and thermal transport in undoped $KTaO_3$, Journal of Physics: Condensed Matter. 6 (1994) 4077-4092, https://doi.org/10.1088/0953-8984/6/22/007.
21. S. Zlotnik, P.M. Vilarinho, M.E.V. Costa, J.A. Moreira, A. Almeida, Growth of Incipient Ferroelectric KTaO3 Single Crystals by a Modified Self-Flux Solution Method, Crystal Growth & Design*- 10 (2010) 3397-3404, https://doi.org/10.1021/cg100036v.
22. G. Müller, The Czochralski Method - where we are 90 years after Jan Czochralski´s invention, Cryst. Res. Technol. 42 (2007) 1150–1161, https://doi.org/10.1002/crat.200711001.
23. D.M. Hannon. Electron Paramagnetic Resonance of Fe^{3+} and Ni^{3+} in $KTaO_3$. Physical Review. 164 (1967) 366. https://doi.org/10.1103/PhysRev.164.366
24. R.C. Miller, W.G. Spitzer, Far Infrared Dielectric Dispersion in $KTaO_3$, Phys. Rev. 129 (1963) 94-98, https://doi.org/10.1103/PhysRev.129.94.
25. W.G. Nilsen, J.G. Skiner, Raman Spectrum of Potassium Tantalate, J. Chem. Phys. 47 (1967) 1413–1418, https://doi.org/10.1063/1.1712096.
26. S. Husain, A.O.A. Keelani. Structural Properties and Williamson-Hall Analysis of Mn Doped $SmFeO_3$. Mater. Today Proc. 5, 5615–5622 (2018). https://doi.org/https://doi.org/10.1016/j.matpr.2017.12.153.
27. J. Madhavi. Comparison of average crystallite size by X-ray peak broadening and Williamson–Hall and size–strain plots for VO^{2+} doped ZnS/CdS composite nanopowder. SN Appl. Sci. 1, 1509 (2019). https://doi.org/10.1007/s42452-019–1291-9.
28. A. Goktas, A. Tumbul, Z. Aba, A. Kilic, F. Aslan. Enhancing crystalline/optical quality, and photoluminescence properties of the Na and Sn substituted ZnS thin films for optoelectronic and solar cell applications; a comparative study. Optical Materials 107 (2020) 110073. https://doi.org/10.1016/j.optical.2020.110073.